minerals

MDPI

Article

Cementation Processes of Cenozoic Reef Carbonates: Insights from Well NK1, Nansha Islands, South China Sea

Zeyi Wei [1,2], Yang Lu [1] and Wen Yan [1,2,*]

[1] State Key Laboratory of Tropical Oceanography, Key Laboratory of Ocean and Marginal Sea Geology, South China Sea Institute of Oceanology, Chinese Academy of Sciences, Guangzhou 511458, China
[2] University of Chinese Academy of Sciences, Beijing 100049, China
* Correspondence: wyan@scsio.ac.cn

Abstract

Carbonate cements record critical information about diagenetic fluid properties and environmental evolution. Carbonate successions in Well NK1 penetrate a depth of 997.7 m, located at Meiji Reef in the Nansha Islands, South China Sea, providing an ideal archive for studying cement characteristics and cementation processes. This study utilized polarizing microscopy, scanning electron microscopy, fluorescence microscopy, and electron probe microanalysis to characterize cement mineralogy, petrography, and geochemistry. The results show that reef cements are dominated by magnesian calcite and dolomite. Magnesian calcite cements include four types: fibrous, columnar-fibrous, bladed, and isopachous. Dolomite cements comprise zoned dolomite (core–rim structured and oscillatory-zoned) and non-zoned dolomite. Fibrous, columnar-fibrous, and bladed magnesian calcite cements occur predominantly in the Meiji and Liyue formations; non-zoned dolomite is mainly developed in the Yongshu and Nanwan formations; and isopachous magnesian calcite and zoned dolomite are primarily found in the Nansha Formation. Isopachous magnesian calcite contains higher MgO (average 3.26 wt%) than fibrous, columnar-fibrous, and bladed types (average 1.39 wt%). The degree of order of dolomites ranges from 0.24 to 0.77 with average of 0.43. Comprehensive analysis indicates three cementation processes: (1) bladed, fibrous, and columnar-fibrous magnesian calcite cements formed during marine cementation; (2) non-zoned dolomite cements formed during seepage-reflux dolomitization from slightly evaporated seawater; and (3) isopachous magnesian calcite and zoned dolomite cements formed during marine phreatic stage. This study reveals the vertical differentiation of reef cement types and provides a petrographic and geochemical basis for understanding the evolution of diagenetic fluids and cementation processes in the Cenozoic reef succession of the Nansha Islands.

Keywords: reef; cement; cementation processes; dolomitization; diagenetic environment; South China Sea

Academic Editor: Olev Vinn

Received: 28 September 2026
Revised: 5 November 2026
Accepted: 16 November 2026
Published: 18 November 2026

Copyright: © 2026 by the authors. Licensee MDPI, Basel, Switzerland. This article is an open access article distributed under the terms and conditions of the Creative Commons Attribution (CC BY) license.

1. Introduction

Cementation is a fundamental component of carbonate diagenesis, referring to the physicochemical and biochemical precipitation of minerals from pore waters that lithify loose sediments into rock [1,2]. The mineralogy, crystal morphology, and geochemical composition of these cements effectively record the properties of diagenetic fluids and the evolution of diagenetic environments [3,4]. Consequently, characteristics of cement are

widely applied to paleo-diagenetic environment, diagenetic fluid, and hydrocarbon reservoir [5]. In reef carbonates, cements primarily include magnesian calcite, aragonite, and dolomite [4]. The genesis and distribution of these cements not only control the degree of reef lithification but also intrinsically link to the depositional and diagenetic evolution [6,7], providing critical insights for diagenetic environment [8].

Research of carbonate cement has evolved from morphological descriptions to high-resolution geochemical analyses. Early studies focused primarily on petrographic classification [9], subsequently establishing hydrogeological models based on pore-fluid dynamics, for example, marine phreatic, meteoric vadose, meteoric phreatic, and mixing zones [10]. With the development of advanced geochemical techniques, stable isotopes (C, O), strontium isotopes, trace elements, and cathodoluminescence (CL) have been widely applied to cement genesis studies, effectively constraining diagenetic fluid sources and diagenetic temperatures [11,12].

Carbonate cement research has progressively developed high-resolution microanalytical approaches. Jones conducted a series of studies on micrometric stoichiometric variations in dolomite crystals from the Cayman Islands, discovering that dolomite precipitation stages can be characterized by zonation features [13]. Techniques such as electron probe microanalysis (EPMA) and laser ablation inductively coupled plasma mass spectrometry (LA-ICP-MS) have revealed rare earth element (REE) variations from crystal cores to rims, documenting continuous shifts in fluid chemistry during dolomitization [14]. Furthermore, multi-proxy analyses combining SEM, CL, and Nano-SIMS suggest that crystal zonation is governed by fluid changes at the reaction interface, reflecting a progressive homogenization between the precipitating mineral and the diagenetic fluid [15]. Clumped-isotope techniques, serving as paleothermometers, have been used to reconstruct diagenetic temperatures and fluid compositions [16]. In situ U-Pb dating techniques have enabled direct determination of carbonate cement formation ages [17,18].

In the South China Sea region, diagenetic studies of reef carbonates began with scientific drilling in the Xisha Islands during the 1970s. Research on wells XK1 and XY2 revealed that diagenesis of reefs in the Xisha Islands involves compaction, marine cementation stage, dissolution, and cementation, with identification of multiple cement types including acicular aragonite, fibrous cement, granular calcite cement, and meniscus calcite cement [19,20]. These features have allowed for the differentiation of marine and meteoric diagenetic environments [21].

In the Nansha Islands, studies on Well NY-2 at Yongshu Reef identified alternating dolomite sequences formed via mixed-water dolomitization influenced by volcanic activity [22]. Previous investigations of Well NK1 at Meiji Atoll have further constrained the dolomitization processes through geochemical and isotopic analyses. Guo et al. [23] integrated clumped-isotope thermometry, petrographic observations, carbon and oxygen isotope data, and trace-element analyses of core samples collected from depths of approximately 1 km to estimate temperatures during shallow-burial diagenesis. They suggested that dolomitization during the late Neogene was associated with evaporative fluids and brine reflux. Focusing on the Lower Nanwan Formation, Luo et al. [12] combined in situ LA-ICP-MS U–Pb dating with elemental and whole-rock geochemical analyses to distinguish island dolostones of multistage diagenetic fluid. They determined that replacement dolomitization occurred between 8.5 and 1.10 Ma, whereas dolomite cement precipitation took place between 8.5 and 6.0 Ma. Additionally, significant meteoric alteration is associated with exposed surfaces [24], while the lower Nanwan Formation preserves evidence of multi-stage selective dolomitization by seawater [12]. Han et al. [25], based on whole-rock elemental compositions, carbon and oxygen isotope data, and iron isotope analyses from Well NK-1, preliminarily proposed that ferroan dolomite formation on Meiji Reef, Nansha Islands, occurred under low-temperature, shallow-burial conditions influenced

by meteoric freshwater leaching, and that this dolomite could serve as an indicator of low sea level. Collectively, these studies have provided important constraints on the timing and fluid conditions of dolomitization in Well NK1.

Previous studies have primarily focused on the timing of dolomitization, fluid sources, and early diagenetic temperatures, while relatively little attention has been paid to in situ microscale analyses or to distinguishing carbonate cements from micritic components. In particular, the relationships between cement morphology and banding patterns, their stratigraphic distribution, and compositional variations within the lithostratigraphic framework of Well NK1 remain poorly understood. Moreover, magnesian calcite and dolomite cements have not been systematically examined together within a unified stratigraphic framework to establish how their petrographic and compositional characteristics vary among different stratigraphic intervals and how these variations relate to distinct diagenetic environments. More broadly, research on carbonate cements in the southern Nansha Islands remains limited, with few systematic investigations of their microscopic characteristics, cement types, and relationships with the evolution of the sedimentary environment. The Well NK1 at Meiji Atoll is the first scientific well in the Nansha Islands, recovering 997.7 m reef carbonates [26]. This core provides ideal material for a systematic study of reef cementation. Accordingly, this study investigates the coral reef carbonates of Well NK1, Nansha Islands. This study focuses on reef carbonate from the Well NK1 at Meiji Reef in the Nansha Islands, South China Sea, which is significant for enriching understanding of reef diagenesis and establishing correspondences between cementation and diagenetic environments.

2. Geological Setting

The South China Sea (SCS), the largest marginal sea in the western Pacific, preserves a complex geological record derived from the interactions among three major lithospheric plates: the Eurasian, Indo-Australian, and Pacific plates [27]. The study area is located at the southwestern margin of the South China Sea Basin, northeast of the Nanhua Waterway (Figure 1). It is bounded to the east by the Palawan Continental Terrane, to the north by the Southwest Sub-basin of the SCS, and to the south by the Borneo Block, with its structural framework controlled by the Northwest Palawan Trough and the Balabac Fault [28]. Tectonically, the area lies within the continental slope fault-step zone of the southern SCS. Characterized by highly attenuated continental crust, this region is widely referred to as the "Dangerous Grounds". Meiji Reef, which exhibits a distinctive rectangular morphology, is located in the central Dangerous Grounds between the Liyue Basin and the Taiping Uplift [29].

The Well NK1, completed at Meiji Reef in the Nansha Islands in 2017, successfully penetrated a 997.7 m thick reefal succession overlying Mesozoic volcanic basement, achieving an average core recovery rate of 91%. A comprehensive chronostratigraphic framework for the well was established through the integration of strontium isotope stratigraphy, magnetostratigraphy, and LA-ICP-MS carbonate U-Pb dating [26,30]. Strontium isotope data indicate that reefal deposition initiated at approximately 26 Ma, a date slightly older than the onset of reef growth in the Xisha Islands. Biostratigraphic analysis of calcareous nannofossils and foraminifera identified seven key marker horizons, revealing depositional sequence spanning the Early Miocene to the Pleistocene [31]. The stratigraphic record is punctuated by a ~9 Myr sedimentary hiatus during the Middle Miocene (ca. 20–11 Ma), which is attributed to regional tectonic uplift of the central Nansha Block [32].

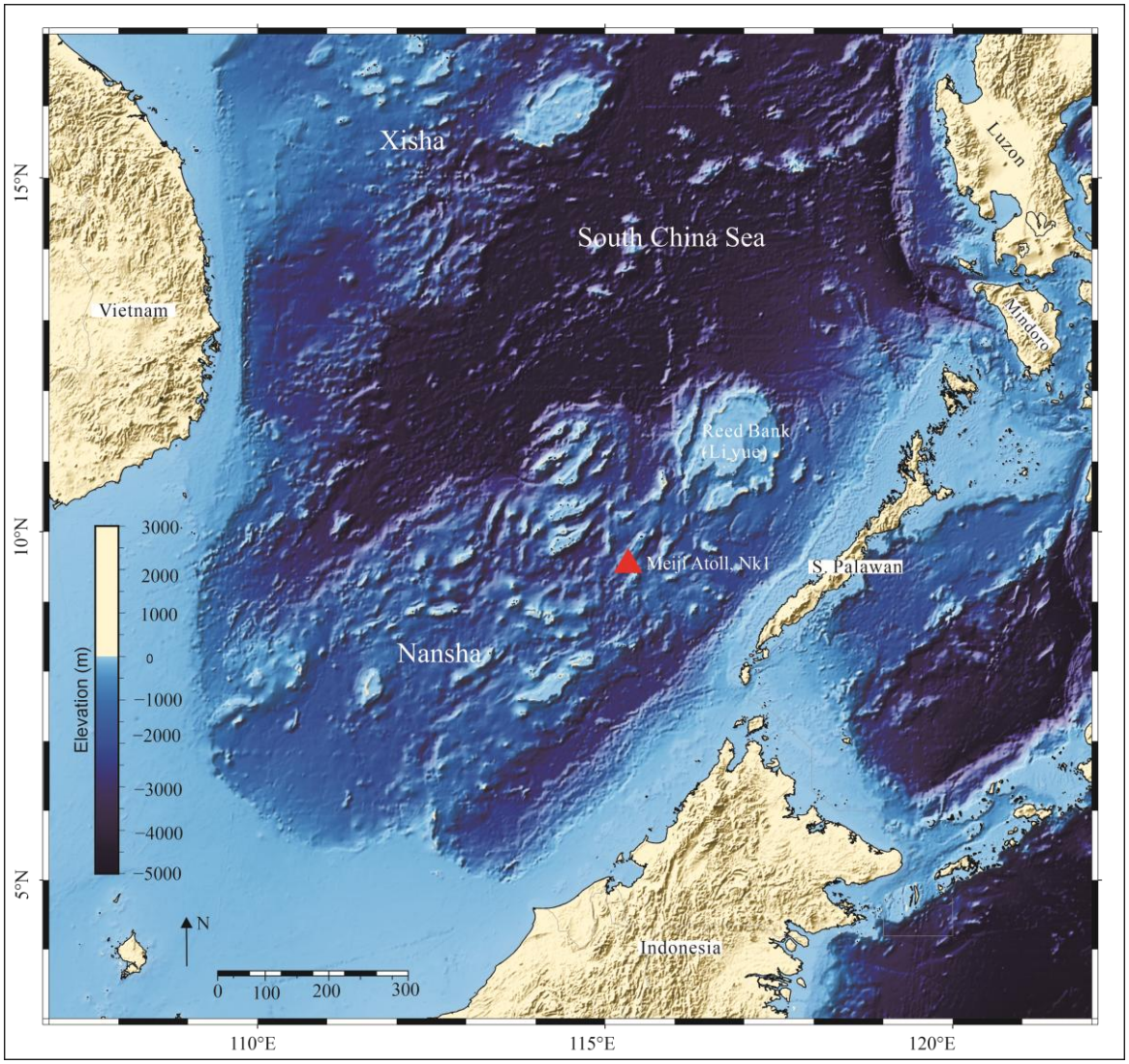


Figure 1. Geographic location of Meiji atoll.

3. Samples and Methods

Based on previous results of the Well NK1, and considering mineralogical characteristics and degree of order of dolomites, a total of 37 rock samples were systematically collected while avoiding biological components, from which 54 thin sections were prepared. The thin sections were prepared as uncovered, polished thin sections impregnated with fluorescent epoxy resin at the Key Laboratory of Ocean and Marginal Sea Geology, South China Sea Institute of Oceanology, Chinese Academy of Sciences. A multi-stage observation was employed to select samples for high-resolution geochemical analysis. Following hand specimen observation and standard optical petrography, thin sections were further characterized by using scanning electron microscopy (SEM) and fluorescence microscopy. Based on these observations, 16 representative samples in which cement is well developed were selected for electron probe microanalysis (EPMA).

X-ray diffraction (XRD) measures the integrated intensities of the dolomite (015) and (110) reflections using X'pert MPD Pro (Malvern Panalytical, Almelo, Netherlands), which serve as the standard proxy for calculating the degree of order of cation. The degree of order of dolomites is determined by calculating the ratio of the (015) peak intensity to the (110) peak intensity [33]. A total of 1205 samples were collected from dolomite intervals. XRD analysis of the samples was examined at the State Key Laboratory of Geological Processes and Mineral Resources, China University of Geosciences (Wuhan). Petrographic

observations were conducted using a Leica DM2700 polarizing microscope (Leica Microsystems CMS GmbH, Wetzlar, Germany) at the Key Laboratory of Ocean and Marginal Sea Geology, South China Sea Institute of Oceanology, CAS. Fluorescence microscopy was performed using Zeiss Axio Scope A1 fluorescence microscope at the Key Laboratory of Tropical Marine Bio-resources and Ecology, CAS. Fluorescence observations were performed on a Zeiss Axio Scope A1 upright epifluorescence microscope (Carl Zeiss, Jena Germany). For blue-light fluorescence imaging of organic matter, the excitation filter was BP 460–490 nm, dichroic mirror 500 nm, and long-pass emission filter LP 510 nm (emission > 510 nm). Images were acquired using Zeiss Zen 3.8 with consistent exposure settings. High-resolution textural characterization was carried out on uncoated, polished thin sections using a Phenom XL G5 desktop scanning electron microscope ((PhenomWorld B.V., Eindhoven, Netherlands) at the Southern University of Science and Technology. Backscattered electron (BSE) imaging was performed under low-vacuum conditions (60 Pa) with an accelerating voltage of 15 kV. Quantitative elemental analyses (Mg, Ca, Mn, and Fe) were conducted using a JEOL JXA-8530F Electron Probe Micro Analyze (JEOL Ltd., Akishima, Tokyo, Japan) at the Testing Center of Sun Yat-sen University. The instrument was operated at an accelerating voltage of 15 kV and a beam current of 20 nA, using a defocused beam diameter of 5 μm. Natural calcite and dolomite were used as calibration standards, yielding detection limits of approximately 100 ppm for manganese (Mn) and iron (Fe). A total of 103 spot analyses were performed on specific cements, including 36 spots on magnesian calcite and 67 spots on dolomite.

4. Results

4.1. Lithology

The Well NK1 consists of Liyue Formation, Meiji Formation, Nanwan Formation, Yongshu Formation, Nansha Formation, and Nanhai Formation (Figure 2). The thickness of reef carbonate is approximately 997.7 m and unconformably overlies Upper Triassic volcanic basement rocks. Carbonate deposition commenced during the late Oligocene (25.8 Ma) and continued into the Quaternary [23].

The Late Triassic volcanic basement mainly consists of dacite and basalt, and is conformably overlain by the Liyue Formation.

The Liyue Formation is a total thickness of approximately 380.5 m, ranging the depth from 997.70 m to 616.50 m. Based on lithological variations, the formation can be divided into three members. The sedimentary sequence is punctuated by 21 identified unconformity surfaces. The formation is an unconformity overlain by the Meiji Formation. The lower member (997.7–885.6 m) is dominated by grayish-white grainstones intercalated with volcanic pebbles. The granular fraction is composed of bioclasts, primarily benthic foraminifera, algae, and minor coral skeletal debris, exhibiting poor to moderate sorting. The core is generally friable and porous, characterized by extensively developed moldic porosity. The Middle Member (885.6–667 m) consists of grayish-white to grayish-yellow rudstones intercalated with framestones, marking the initial appearance of variegated sedimentary facies. The biotic assemblage is notably more diverse, commonly containing coral frameworks, gastropods, bivalves, and algal fossils. The Upper Member (667–616.5 m) is composed primarily of grayish-white to grayish-brown coral framestones and rudstones, rich in dendroid skeleton and massive reefal frameworks. The algal flora includes coralline and stromatolitic forms. Localized reddish-brown staining is observed, and the formation is in unconformable contact with the overlying Meiji Formation.

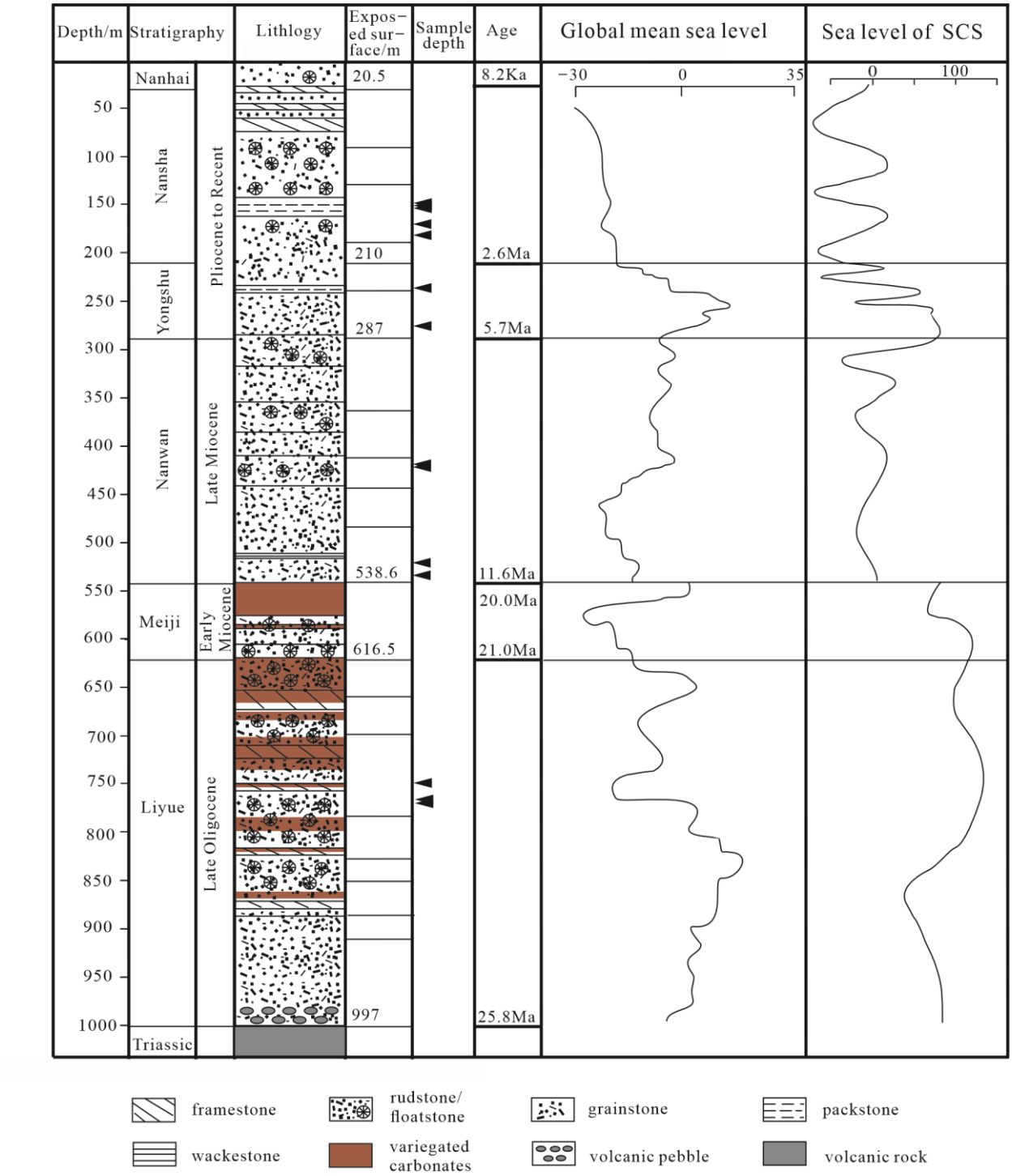


Figure 2. Lithostratigraphic unit division of Well NK1 (adapted from [26]).

The Meiji Formation is approximately 77.9 m, ranging from 616.5 to 538.6 m. Five exposure surfaces have been identified within it. The lithology is composed primarily of grainstone and wackestone. The uppermost member is characterized by the development of variegated limestone, possibly indicating a period of fluctuating redox conditions or subaerial weathering. The formation terminates with an unconformable contact with the overlying Nanwan Formation.

The Nanwan Formation ranges from 538.6 to 287 m in depth and represents the principal dolostone interval. The lithology is dominated by rudstone and grainstone, and can be divided into upper and lower members. The lower member (538.6–384.98 m) consists of grayish-white to grayish-yellow grainstone, with well-developed corals and algae.

Dissolution pores and cavities are moderately developed. The upper member (384.98–287 m) contains completely dolomitized intervals, with lithology characterized by alternating grayish-white to grayish-yellow rudstone and grainstone.

The Yongshu Formation is approximately 77 m thick, ranging from 287 to 210 m in depth. The lithology is dominated by grayish-white to grayish-yellow grainstone and wackestone, with a relatively high abundance of planktonic foraminifera, including corals, gastropods, and algae. This formation is in unconformable contact with the overlying Nansha Formation.

The Nansha Formation ranges from 210.1 to 20.5 m in depth. The lithology is dominated by grayish-white to yellowish-white wackestone, rudstone, grainstone, and framestone. The lower member (210–120.5 m) consists of grayish-white to yellowish-white rudstone interbedded with wackestone, with extremely abundant corals. The upper member (120.5–20.5 m) is mainly composed of framestone interbedded with grainstone. Dissolution pores and cavities are extremely well developed, particularly within coral frameworks, forming honeycomb-like vugs and moldic porosity. At least nine major exposure surfaces have been identified in this formation.

The Nanhai Formation is approximately 20 m thick and ranges from 0 to 20.5 m in depth. It consists of loose bioclasts and coral gravel. The lower member (14–20.5 m) gradually transitions into consolidated coral framestone. The upper member (0–14 m) comprises unconsolidated coral rubble and lime mud deposits. The rubble displays mixed sizes with poor sorting.

4.2. Characteristics of Magnesian Calcite Cements

4.2.1. Characteristics of Scanning Electron Microscope of Magnesian Calcite Cements

Based on compositions of mineral, samples of magnesian calcite cements were collected from the Liyue and Nansha formations (Figure 3). Integrated petrographic and scanning electron microscopy (SEM) analyses identified four distinct cement morphologies: columnar-fibrous, fibrous, bladed, and isopachous (Figure 3).

Isopachous magnesian calcite cements precipitates as circumgranular rims around dolomite. The cements occur a comb-like distribution with an essentially uniform thickness of approximately 100–200 μm in all directions (Figure 3a). The cements have a characteristic of sweeping extinction in cross-polarized light (Figure 3b). In certain intergranular pores between algal organisms or skeletal fragments, the isopachous magnesian calcite appears to have disintegrated along micro-fractures to form discrete magnesian calcite. These fragmented particles typically exhibit polygonal shapes with irregular boundaries (Figure 3).

Bladed magnesian calcite cements are characterized by closely arranged crystals with acute pyramidal terminations growing perpendicular to micrite. SEM observations reveal distinct growth zonation and a tapered crystal morphology that widens from the base toward the growth direction (Figure 3c). In cross-polarized light, the cements exhibit high-order white interference colors and sharp contrast to the micrite (Figure 3d).

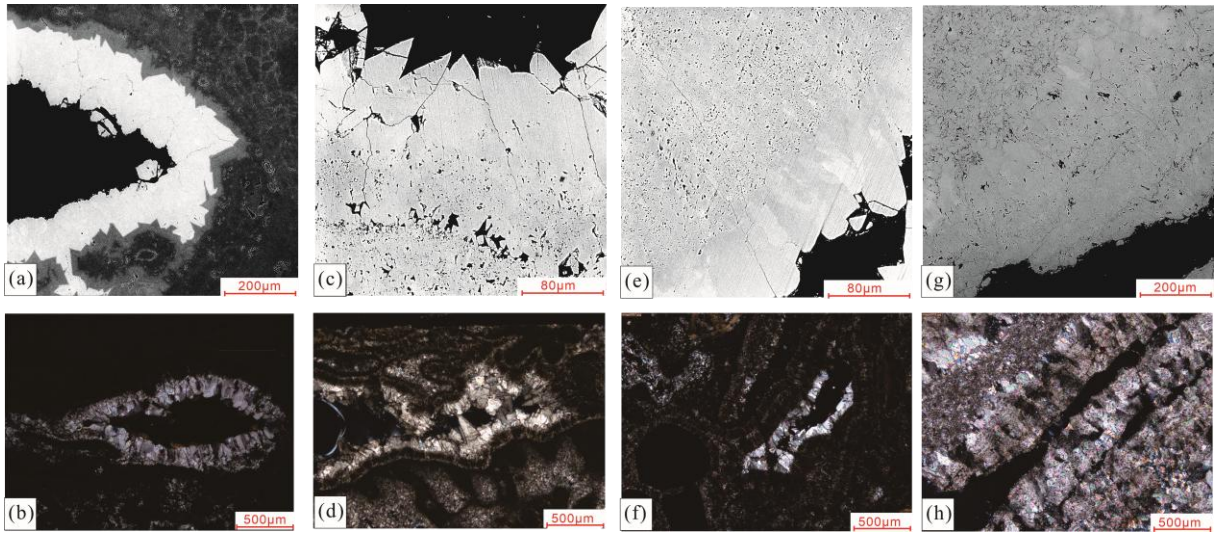


Figure 3. Characteristics of magnesian calcite cements. (**a**) Isopachous magnesian calcite cement in the Nansha Formation, depth 161.86 m, SEM-BSE image, 330×; (**b**) cross-polarized light corresponding to (**a**); (**c**) bladed magnesian calcite cement in the Liyue Formation, depth 773.75 m, SEM-BSE image, 870×; (**d**) cross-polarized light corresponding to (**c**); (**e**) columnar-fibrous magnesian calcite cement in the Liyue Formation, depth 783.75 m, SEM-BSE image, 950×; (**f**) cross-polarized light corresponding to (**e**); (**g**) fibrous cement in the Liyue Formation, depth 749.95 m, SEM-BSE image, 330×; and (**h**) cross-polarized light corresponding to (**g**).

Columnar-fibrous magnesian calcite cements consist of densely packed columnar crystals with sub-parallel sides and uniform dimensions, nucleating on and growing around micrite (Figure 3e). Crystal terminations appear rounded or flat. In cross-polarized light, these aggregates display a sweeping, fan-shaped extinction pattern upon stage rotation (Figure 3f).

Compared to the columnar variety, individual crystals in fibrous magnesian calcite cements are more difficult to resolve optically. SEM imaging shows well-developed crystal faces forming a crust over a dense, uniform micrite (Figure 3g). In cross-polarized light, the crystals display palisade-like cements characterized by inverted V-shaped extinction (Figure 3h).

The distribution of vertical types of cement reveals a distinct vertical zonation. Bladed cements, columnar-fibrous cements, and fibrous cements, which nucleate directly on micrite, are predominantly developed in deeper, calcite-dominated intervals. In contrast, isopachous magnesian calcite cements encrusting dolomite are characteristic of shallower formation.

4.2.2. Characteristics of Electron Probe Microanalysis of Magnesian Calcite Cements

Electron probe microanalysis results demonstrate that the magnesian calcite cements in the study area are chemically pure, with MnO and FeO contents consistently ranging from below detection limits to 0.02 wt%. These negligible concentrations indicate a lack of significant contamination by external Fe- or Mn-rich fluids, suggesting precipitation occurred in an open, oxidizing environment devoid of late-stage ferroan diagenetic alteration.

Based on previous research of mineralogy, representative samples were selected from the Nansha Formation (150.47–163.53 m) and Liyue Formation (749.95–774.00 m) for detailed MgO and CaO analysis Table 1). In the Nansha Formation, samples generally exhibit high MgO values (2.25–4.78 wt%) and relatively lower CaO values (50.51–52.37 wt%). At 150.47 m, MgO ranges from 2.83 to 3.22 wt% (mean 3.08 wt%), while CaO values

range from 50.98 to 51.72 wt% (mean 51.33 wt%); at 152.79 m, MgO ranges from 3.69 to 4.78 wt% (mean 4.28 wt%), CaO values range from 50.51 to 51.89 wt% (mean 50.94 wt%). In contrast, the Liyue formation is characterized by significantly lower MgO (0.90–2.05 wt%) and higher CaO contents (52.23–54.72 wt%). At 749.95 m, MgO values range from 1.22 to 2.05 wt% (mean 1.75 wt%), with CaO values of 52.23–54.09 wt% (mean 52.90 wt%); at 773–774 m, MgO values range from 0.90 to 1.60 wt% (mean 1.16 wt%), and the highest CaO content ranges from 53.30 to 54.72 wt% (mean 53.83 wt%).

Table 1. Electron probe microanalysis results of magnesian calcite cements.

Depth	MgO/wt%	Mean Value of MgO/wt%	CaO/wt%	Mean Value of CaO/wt%	Formation	Types of Magnesian Calcite Cements
150.47 m	2.83–3.22	3.08	50.98–51.72	51.32	Nansha	Isopachous
152.79 m	3.69–4.78	4.28	50.51–51.89	50.94	Nansha	Isopachous
163.53 m	2.25–2.94	2.63	51.05–52.37	51.59	Nansha	Isopachous
150.47–163.53 m	2.25–4.78	3.26	50.51–52.37	51.32	Nansha (Total)	Isopachous
749.95 m	1.22–2.05	1.75	52.23–54.09	52.90	Liyue	Bladed; Columnar fibrous; Fibrous
773–774 m	0.90–1.60	1.16	53.30–54.72	53.83	Liyue	Bladed; Columnar fibrous; Fibrous
749.95–774 m	0.09–2.05	1.39	52.23–54.72	53.46	Liyue (Total)	Bladed; Columnar fibrous; Fibrous

4.3. Characteristics of Dolomite Cement

4.3.1. Characteristics of Scanning Electron Microscopy of Dolomite Cement

Based on mineral compositions, dolomite cement samples were collected from the Nansha, Yongshu, and Nanwan formations. Based on microscopy and scanning electron microscopy, dolomite cements can be classified into two types: zoned dolomite and non-zoned dolomite (Figure 4–6). The zoned dolomite can be further subdivided into core–rim structured dolomite and oscillatory-zoned dolomite based on zonation characteristics.

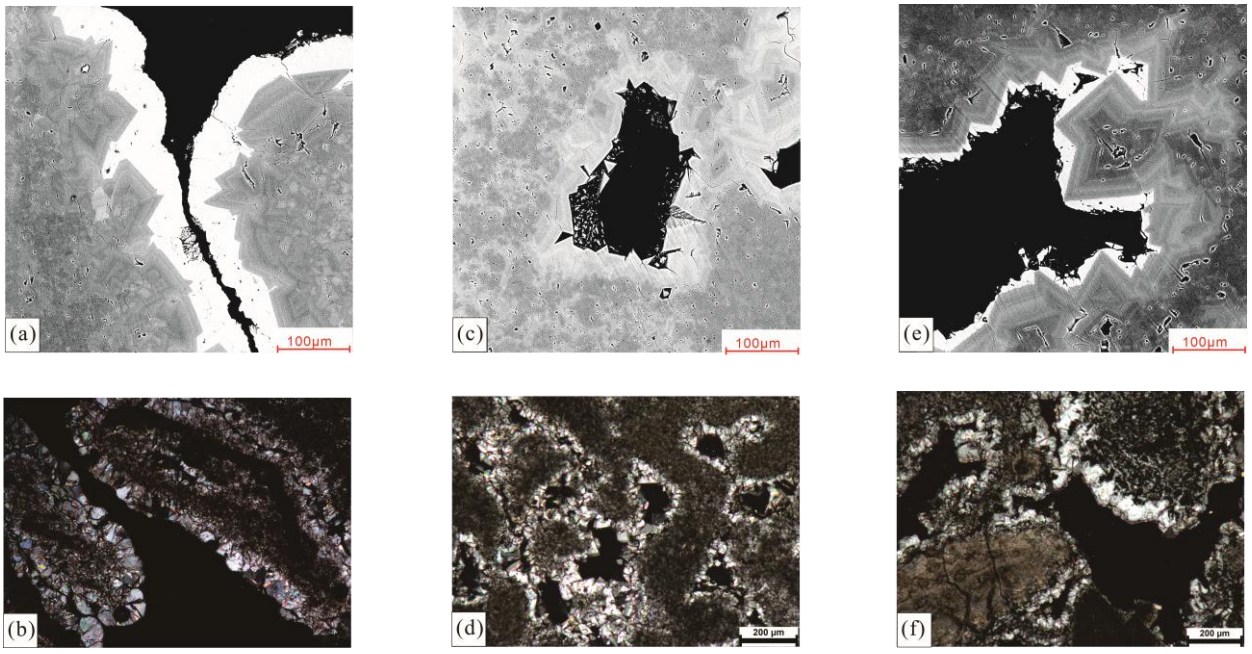


Figure 4. Characteristics of core–rim dolomite cements. (**a**) Nansha Formation, 152.79 m, SEM-BSE image, 570×; (**b**) cross-polarized light corresponding to (a), 5× magnification; (**c**) Nansha Formation,

depth 176.03 m, SEM-BSE image, 710×; (**d**) cross-polarized light corresponding to (**c**); (**e**) Nansha Formation, depth 179.28 m, SEM-BSE image, 790×; and (**f**) cross-polarized light corresponding to (**e**).

Dolomite cements exhibit stronger euhedral character than magnesian calcite in SEM. The core–rim structure is characterized in backscattered electron images by dark gray cores surrounded by light gray rims (Figure 4a,c,e), also commonly referred to as cloudy-core–clear-rim texture. Petrographically, the cores are typically composed of dark micrite, whereas the columnar rims develop well-formed, straight, and sharp crystal faces, imparting an overall euhedral to subhedral morphology to the crystals. In cross-polarized light, the rims display distinct extinction, contrasting with the turbid cores (Figure 4b,d,f).

Oscillatory-zoned dolomite is defined by fine-scale rhythmic banding. In BSE images, this texture manifests as multiple alternating light and dark concentric layers on a micrometer scale (1–10 μm; Figure 5a), while optical microscopy reveals a gross morphology similar to the core–rim structure, often displaying continuous, regular concentric rhombohedral zones with planar faces (Figure 5b). Under cross-polarized light, the intricate, fine-scale compositional zonation resolved by BSE cannot be distinguished (Figure 5b,d).

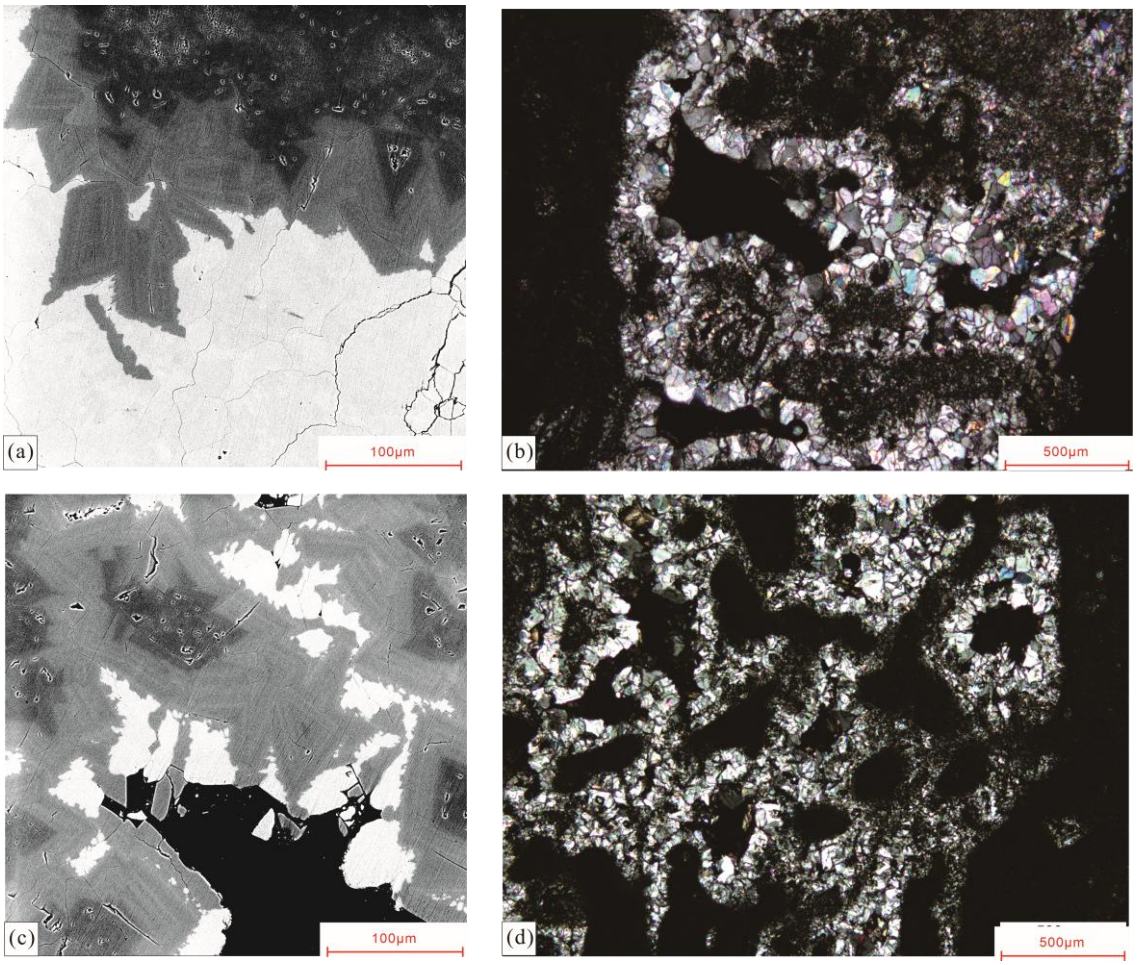


Figure 5. Characteristics of oscillatory-zoned cements. (**a**) Nansha Formation, 163.53 m, SEM-BSE image, 810×; (**b**) cross-polarized light corresponding to (**a**), 2.5× magnification. (**c**) Nansha Formation, depth 163.53 m, SEM-BSE image, 800×; and (**d**) cross-polarized light corresponding to (**c**), 2.5× magnification.

Non-zoned dolomite is characterized by a homogeneous texture with uniform gray-scale intensity in BSE images, lacking either core–rim or oscillatory zonation patterns

(Figure 6). The sizes of crystals approximately range from 20 to 100 μm and exhibit a range of morphologies from euhedral to anhedral. They display uniform extinction, appearing as discontinuous cement phases in microscopy.

The two types of dolomite cements also show differences in vertical distribution. The shallow stratum (150.47–163.53 m) is dominated by dolomite with clear zonation, with specific occurrences of oscillatory-zoned dolomite at 163.53 m. In contrast, the deeper stratum (from 234.43 m) is characterized exclusively by non-zoned dolomite, with no further occurrence of zoned varieties.

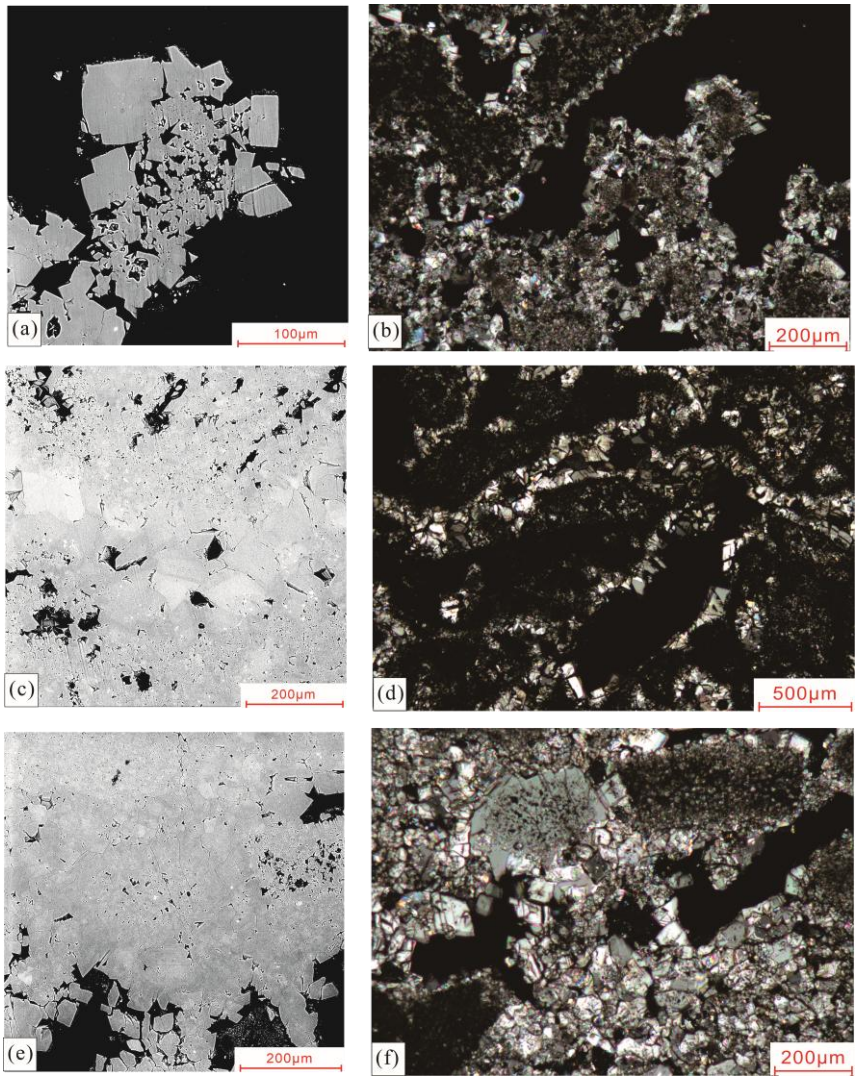


Figure 6. Characteristics of non-zoned dolomite cements. (**a**) Yongshu Formation, 234.43 m, SEM-BSE image, 840×; (**b**) cross-polarized light corresponding to (**a**), 5× magnification; (**c**) Nanwan Formation, depth 425.73 m, SEM-BSE image, 390×; (**d**) cross-polarized light corresponding to (**c**); (**e**) Nanwan Formation, depth 529.23 m, SEM-BSE image, 400×; and (**f**) cross-polarized light corresponding to (**e**).

4.3.2. Characteristics of Electron Probe Microanalysis of Dolomite Cement

The dolomite cements contain negligible concentrations of trace elements, with MnO and FeO contents ranging from 0.00 to 0.04 wt% and 0.00 to 0.03 wt%, respectively. Based on the electron probe microanalysis results, the study formations can be divided into four depths: 150.47–163.53 m, 176.03–180.83 m, 234.43–276.33 m, and 419.83–534.24 m.

Contents of MgO vary across these intervals: the 150.47–163.53 m interval shows a range of 16.84–19.89 wt% (mean 18.05 wt%); the 176.03–180.83 m interval shows 16.19–22.33 wt% (mean 18.28 wt%); the 234.43–276.33 m interval displays higher values of 17.72–20.59 wt% (mean 19.43 wt%); and the deeper 419.83–534.24 m interval ranges from 17.49 to 18.86 wt% (mean 18.06 wt%).

The corresponding contents of CaO are as follows: 31.18–34.38 wt% (mean 32.91 wt%) at 150.47–163.53 m; 30.87–36.13 wt% (mean 33.27 wt%) at 176.03–180.83 m; a lower range of 29.43–32.76 wt% (mean 30.88 wt%) at 234.43–276.33 m; and 32.18–33.81 wt% (mean 33.30 wt%) at 419.83–534.24 m.

Detailed analysis of zoned dolomite within the 150.47–180.83 m interval reveals distinct compositional differences between bands (Table 2). Bright bands are characterized by MgO contents of 16.19–18.15 wt% (mean 17.29 wt%) and CaO contents of 32.78–35.02 wt% (mean 33.49 wt%). In contrast, dark bands exhibit MgO contents of 16.99–22.33 wt% (mean 18.49 wt%) and CaO contents of 30.87–36.13 wt% (mean 32.85 wt%). Non-zoned dolomite displays MgO contents ranging from 17.49 to 20.59 wt% (mean 18.29 wt%) and CaO contents from 29.43 to 33.81 wt% (mean 32.90 wt%).

Table 2. Electron probe microanalysis results of dolomite cements.

Depth	MgO/wt%	Mean Value of MgO/wt%	CaO/wt%	Mean Value of CaO/wt%	Formation	Types of Dolomite Cements
150.47–180.83 m	16.19~18.15	17.29	32.78~35.02	33.49	Nansha	Bright bands of zoned dolomite cements
150.47–177.23 m	16.99~22.33	18.49	30.87~36.13	32.85	Nansha	Dark bands of zoned dolomite cements
150.47–163.53 m	16.84~19.89	18.05	31.18~34.38	32.91	Nansha	Zoned dolomite cements
176.03–180.83 m	16.19~22.33	18.28	30.87~36.13	33.27	Nansha	Zoned dolomite cements
234.43–276.33	17.72~20.59	19.43	29.43~32.76	30.88	Yongshu	Non-zoned dolomite cements
419.83–534.24	17.49~18.86	18.06	32.18~33.81	33.30	Nanwan	Non-zoned dolomite cements
234.43–534.24 m	17.49~20.59	18.29	29.43~33.81	32.9	Yongshu and Nanwan (Total)	Non-zoned dolomite cements

4.4. Characteristics of Fluorescence Microscopy

The carbonate samples exhibit heterogeneous fluorescence characteristics that correlate with specific petrographic components in blue light. Pore is non-fluorescent, appearing in black areas. Similarly, isopachous magnesian calcite cements are essentially non-fluorescent. Both magnesian calcite and dolomite cements generally appear grayish-black (Figure 7a,c), although weak blue light appear at the margins of intergranular pores (Figure 7a). The micrite displays moderate fluorescence intensity, clearly different from the non-fluorescent cements in blue light (Figure 7b,d). In the multi-generation marine sediments of the Liuyang Formation, distinct fluorescent patterns were observed along the fractures of the cement (Figure 7e). Notably, the grayish-brown cements display rhythmic

growth zonation characterized by alternating wide bright bands and narrow dark bands in cross-polarized light (Figure 7f).

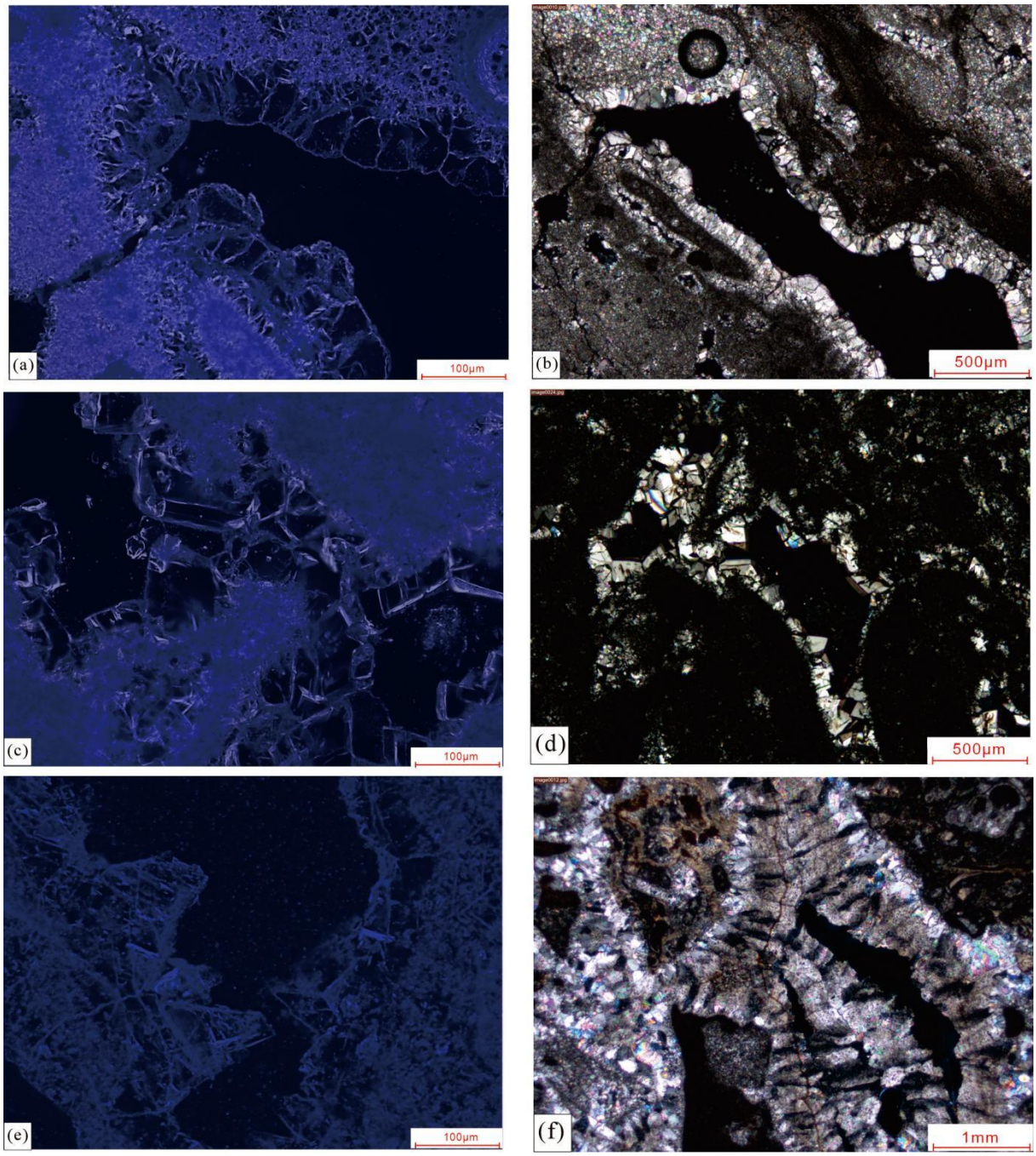


Figure 7. Characteristics of fluorescence microscopy. (**a**) Nansha Formation, depth 152.79 m, blue-light fluorescence; (**b**) cross-polarized light corresponding to (**a**); (**c**) Nanwan Formation, depth 424.93 m, blue-light fluorescence; (**d**) cross-polarized light corresponding to (**c**); (**e**) Liyue Formation, depth 749.95 m, blue-light fluorescence; and (**f**) cross-polarized light corresponding to (**e**).

4.5. Degree of Order of Dolomites

To characterize the fluid properties driving dolomitization, the interval exhibiting the most intense dolomitization (120.77–537.43 m) was selected for detailed analysis. Data from 120.77 to 537.43 m are considered most representative of the dolomitizing fluids. The degree of order of dolomites varies from 0.235 to 0.772, with a mean value of 0.426. Based on these variations (Figure 8), five segments can be identified: 120.77–171.43 m with values

of 0.235–0.522 (average 0.364); 171.43–230.43 m with values of 0.358–0.683 (average 0.536); 230.43–245.03 m with values of 0.303–0.457 (average 0.395); 245.03–301.73 m with values of 0.772–0.264 (average 0.583); and 301.73–537.43 m with values of 0.266–0.647 (average 0.403).

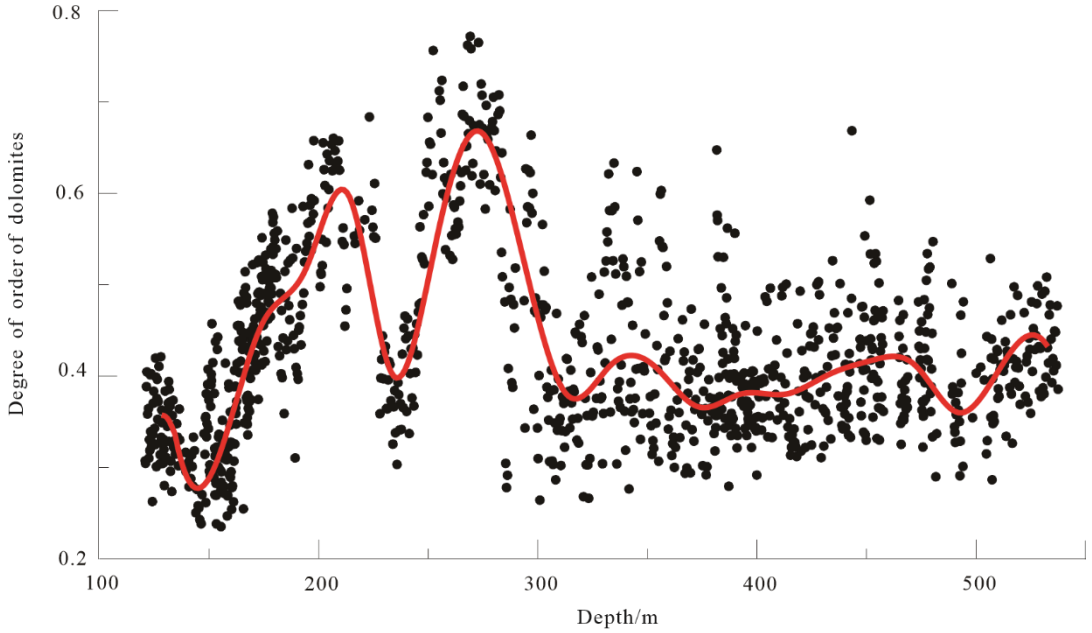


Figure 8. Degree of order of dolomites (120.77–537.43 m) in Well NK1. The black dots represent measured samples; the red line represents the smoothed trend of degree of order.

5. Discussion

5.1. Genesis of Magnesian Calcite Cements

The Nansha Formation (150.47–163.53 m) exhibits isopachous magnesian calcite cements and dolomite. In cross-polarized light, sweeping extinction patterns are observed. Two types of magnesium calcite are identified. The first type is comb-like crusts directly on dolomite cements, with thicknesses of approximately 100–200 μm. The second type is irregularly distributed along dolomite cements and exhibits embayed dissolution margins under the microscope. Electron probe microanalysis reveals that the comb-like type MgO is 3.08 wt% at 150.47 m, whereas the dissolved type MgO is 4.28 wt% at 152.79 m.

Microscopic observations reveal that the margins of zoned dolomite crystals are enveloped by continuous, isopachous magnesian calcite cement rims, which also occur along the surfaces of dolomite cements. This distribution indicates that the magnesian calcite is not merely a replacement product confined to the margins of dolomite, but rather a pore-filling cement precipitated within pores. The internal bright and dark bands of the dolomite are well preserved, and the contact between magnesian calcite and dolomite is planar, with no discernible evidence of truncation (Figure 4). These features indicate that the zoned dolomite formed prior to the precipitation of magnesian calcite. The isopachous distribution of magnesian calcite along the surfaces of different grains suggests that the pores were water-saturated during cement precipitation. This cement is a diagnostic indicator of marine phreatic diagenesis and indicates water-saturated condition [34].

The second type of magnesian calcite cement rim is characterized by irregularly missing segments and embayed depressions, indicating that it underwent dissolution after its formation. Given the geological context of multiple episodes of sea-level fall and depositional exposure in the study area, this dissolution may have been associated with meteoric freshwater percolation during subaerial exposure of the reef. Magnesian calcite is more

susceptible to dissolution than low-Mg calcite and may therefore have undergone preferential dissolution under the influence of meteoric freshwater [35].

EPMA indicates extremely low MnO and FeO contents in the magnesium calcite, with most values below detection limits. It excludes significant influence from external Fe- and Mn-rich fluids. Fluorescence microscopy shows the cement appears gray-black with non-fluorescent or weakly fluorescent characteristics, contrasting sharply with the moderate fluorescence of micrite. The lack of fluorescence suggests formation within an oxidizing or weakly reducing marine diagenetic environment devoid of organic matter participation [36,37]. The preservation of isopachous magnesium calcite cements implies later stage of the cementation process relatively confined marine conditions [38].

The Meiji and Liyue Formations have fibrous, columnar-fibrous, and bladed magnesium calcite cements. EPMA results indicate MgO contents of 1.75 wt% at 749.95 m and 1.16 wt% at 773–774 m, suggesting the cements are predominantly low-magnesium calcite. In cross-polarized light, crystals radiate outward from original nucleation sites with irregular boundaries. Cement growth occurred along micrite, forming crusts that record multiple stages of diagenetic evolution. Fluorescence microscopy reveals that magnesium calcite cements in the Liyue Formation exhibit weak fluorescence near pore margins, attributed to abundant large benthic foraminifera and coralline algae debris. However, the bulk of the cement displays negligible fluorescence, indicating that organic matter did not significantly participate in the cementation processes. Grayish-brown fractures traverse cements, suggesting the presence of organic acids within pore fluids [39]. The cements precipitated from seawater where calcium carbonate was supersaturated. Initially, high magnesium calcite and aragonite precipitated directly from seawater. During burial along steep reef margins, sustained contact with seawater facilitated the gradual transformation of metastable phases into stable low-magnesium calcite [40,41].

Fibrous, columnar-fibrous, and bladed calcite cements are predominantly developed in the Meiji and Liyue formations, whereas isopachous magnesian calcite cements are characteristic of the Nansha Formation. The Meiji and Liyue intervals correspond to rapid reef aggradation and are characterized by active seawater circulation. Relatively high-flow energy and carbonate supersaturation may have promoted rapid nucleation and crystal growth, favoring the development of fibrous and columnar morphologies [1]. In contrast, the development of isopachous magnesian calcite cements in the Nansha Formation coincides with reef progradation [42,43]. These contrasting cement morphologies may reflect differences in pore-water exchange, carbonate saturation states, and crystal growth conditions associated with changes in reef development. In the Nansha Formation, seawater could still have entered the pore system and supplied the components required for cement precipitation, while pore-water exchange may have been relatively less vigorous than in the rapidly aggrading Meiji and Liyue intervals. Thus, the development of isopachous cements does not necessarily imply either vigorous convective circulation or complete restriction of pore-water flow. Instead, their occurrence records relatively uniform precipitation under water-saturated marine phreatic conditions. Their direct growth on zoned dolomite further establishes that magnesian calcite precipitation postdated dolomite formation.

5.2. Genesis of Dolomite Cements

Zoned dolomite cements are well developed within the lower Nansha Formation (150.47–163.53 m), characterized by distinct core–rim structures. In backscattered electron imagery, the dolomite cements exhibit dark gray cores surrounded by light gray rims, with the rim portions displaying euhedral to subhedral crystal faces. The dark cores represent micrite, whereas the limpid rims constitute later-stage dolomite cement overgrowths. This textural dichotomy is diagnostic of material redistribution during

dolomitization [11,44,45], reflecting a two-stage kinetic process: (i) Nucleation and Replacement: During early diagenesis, highly supersaturated fluids rapidly replaced primary sediments, generating cloudy micritic cores; (ii) Overgrowth: As fluid supersaturation decreased and reaction times extended, slower precipitation formed the clear dolomite cement rims [12]. Although previous in situ U-Pb dating suggests dolomitization occurred in multiple phases [23], this study focuses specifically on the cementation phase; the genesis of the micritic precursor warrants further investigation.

Oscillatory-zoned dolomite occurs at 163.53 m, consisting of alternating micrometer-scale (1–10 μm) light and dark bands. This morphology represents a transition between the overlying zoned and underlying non-zoned dolomites. Geochemically, the alternating bands reflect periodic fluctuations in pore-fluid chemistry [33]. Electron probe microanalysis (EPMA) reveals that the bright bands possess slightly lower MgO contents (mean 17.29 wt%; 16.19–18.15 wt%) compared to the dark bands (mean 18.49 wt%; 16.99–22.33 wt%). In BSE images, brightness is inversely correlated with magnesium content due to the lower atomic number of Mg relative to Ca; thus, the Ca-enriched bands appear brighter. These compositional variations indicate fluctuations in fluid chemistry during dolomite growth [13,46]. In open diagenetic systems, periodic seawater incursion may drive fluctuations in the fluid Mg/Ca ratio, generating compositional zoning. Conversely, in relatively restricted systems, the consumption of Mg^{2+} during dolomite precipitation may depress the Mg/Ca ratio, which could subsequently be restored through fluid diffusion or replenishment, resulting in the rhythmic repetition of light and dark bands. Comparison with global sea-level curves and regional sea-level reconstructions in the South China Sea indicates that the development of zoned dolomite broadly coincides with intervals of pronounced sea-level fluctuations (Figure 2). Since the late Miocene, Well NK1 has recorded multiple glacial fluctuations, including at least nine Quaternary sea-level changes [12,47]. These sea-level fluctuations may have influenced seawater replenishment and pore-water circulation within the reef framework, thereby modifying pore-fluid chemistry and potentially contributing to the development of compositional zoning. In this context, the precipitation of relatively low-Mg dolomite (bright bands) during highstands and relatively high-Mg dolomite (dark bands) during lowstands may reflect changes in the relative contributions of normal and slightly evaporated seawater. However, this interpretation represents a possible mechanism rather than a uniquely established relationship.

Non-zoned dolomite developed in the lower Yongshu Formation (234.43 m) and the Yongshu Formation. These cements exhibit euhedral–anhedral textures, occasionally displaying irregular edges of partial dissolution–reprecipitation. Previous paleotemperature reconstructions for Well NK1 indicate a shallow burial history characterized by low-temperature dolomitization (18–34 °C) [23]. This thermal regime is consistent with the observed crystal textures, as temperatures remained well below the critical threshold (~50 °C) typically required for the transition from euhedral to anhedral mosaic textures [48]. The genesis of these non-zoned dolomites is attributed to seepage-reflux dolomitization, a primary mechanism for platform-scale dolomitization [33]. In the model, slightly evaporated seawater, having elevated density, percolates downward through the platform, reacting with precursor carbonates. The geochemical signature of dolomitizing fluids in Well NK1 confirms an origin from slightly evaporated seawater [23], providing strong evidence for the seepage-reflux model in the Nanwan and Yongshu Formations.

5.3. Stages of Cementation in Well NK1

Based on the above analysis, different types of cements are the combined result of different diagenetic environments, climatic conditions, and sea-level changes. The process

of cementation of reef carbonates in the study area can be divided into three principal stages (Figure 9).

Marine cementation stage is characterized by the precipitation of bladed, fibrous, and columnar-fibrous magnesian calcite cements, which exhibit low MnO and FeO contents and no to weak fluorescence. During early deposition of reef, pores were completely filled with seawater. The highly supersaturated calcium carbonate in seawater promoted rapid nucleation and crystal growth, forming fibrous morphologies [49]. As pore-water circulation weakened and supersaturation decreased, crystal growth rates slowed, resulting in the transition to bladed morphologies. Multiple processes of cementation are related to supply of periodic fluid [50].

The seepage-reflux stage is characterized by the development of non-zoned dolomite with dolomitization. Dolomitization fluids originated from slightly evaporated seawater [23]. The moderately ordered dolomite formation (301.73–537.43 m, mean degree of order of dolomites 0.40) is located in the main part of the seepage-reflux zone, with sustained stable supply of enriched Mg^{2+} fluids. The highly ordered dolomite formation (245.03–301.73 m, mean degree of order of dolomites 0.58) is located in the upper part of the seepage-reflux zone, representing a relatively slow dolomitization stage. Fluid supply coupled with moderately elevated temperatures facilitated slower crystallization and a higher order of lattice [33]. The homogeneous composition of non-zoned dolomite indicates formation with relatively stable conditions, consistent with a stable supply of high Mg/Ca fluid in the seepage-reflux zone.

The mean degree of cation ordering of dolomite in the 245–301.73 m is 0.58, higher than the average values of the other intervals. Dolomite in this interval predominantly exhibits a sucrosic texture and is interpreted to have formed through replacement. Its Mg/Ca molar ratio is 0.96, indicating a composition close to ideal stoichiometry. The stoichiometric composition and degree of cation ordering of dolomite are controlled by multiple factors. Experimental studies demonstrated that higher fluid Mg/Ca ratios favor the formation of dolomite with compositions approaching ideal stoichiometry, whereas the degree of cation ordering evolves in response to the progress of dolomitization and subsequent structural reorganization [51]. Experiments further showed that both the stoichiometric composition and degree of cation ordering can increase as replacement of the precursor carbonate approaches completion [51]. These results suggest that sustained replacement may have contributed to the development of nearly stoichiometric dolomite and its relatively high degree of cation ordering in this interval. In addition, temperature influences cation diffusion and structural reorganization, thereby affecting the kinetics of dolomite ordering. Based on clumped-isotope, diagenetic alteration of the carbonates in Well NK1, including dolomitization, may have occurred at depths of approximately 200 m below sea level, at temperatures ranging from approximately 15 to 28 °C [23]. Kim et al. [52] suggested that, under near-surface temperature conditions, localized dissolution and reprecipitation driven by changes in fluid saturation can promote dolomite crystal growth and ordering. Thus, prolonged fluid–rock interaction and repeated dissolution–reprecipitation may have progressively enhanced the structural ordering of dolomite.

Marine phreatic stage is characterized by the development of isopachous magnesian calcite and zoned dolomite. Sea-level fluctuations may have influenced the composition and circulation of pore fluids during the marine phreatic stage. During high sea level, enhanced seawater replenishment may have favored the input of normal seawater, whereas during low sea level, changes in hydrological conditions may have increased the relative contribution of slightly evaporated seawater. These variations may have contributed to fluctuations in pore-fluid Mg/Ca ratios and, consequently, the development of alternating bright and dark dolomite bands. The oscillatory-zoned dolomite at 163.53 m represents a transitional type between zoned and non-zoned dolomite. Cementation was

the primary diagenetic process, with seawater flowing along pores and precipitating over prolonged periods to form isopachous magnesian calcite.

Due to sea-level falls, the reef was subjected to subaerial exposure, leading to meteoric leaching and weathering. Prolonged lowstands resulted in intense epigenetic karstification, creating dissolution boundaries on non-zoned dolomites. Subsequent transgression re-submerged the previously exposed carbonates, initiating new cycles of aggradation and marine cementation [51]. Sediment accumulation drove the underlying strata into the marine cementation stage, a stage characterized by compaction, the reduction in primary porosity, and the restriction of pore-water circulation. As overlying sediments accumulated, previously deposited materials underwent marine cementation stage, with primary porosity reduction and gradual weakening of pore water, leading to sediment compaction [40,49]. When sea level rose to water depths suitable for coral growth, the reef resumed vertical aggradation, forming new sedimentary cycles. This periodic sea-level fluctuation created multiple stacked exposure–deposition cycles in the vertical succession. High-frequency sea-level fluctuations induced high-frequency fluctuations in diagenetic fluid chemical composition [37,52], with dolomite cements forming alternating light and dark bands. Each exposure event associated with sea-level fall and reduced precipitation, leading to insufficient freshwater supply, may have resulted in the process of cementation, seepage reflux, and marine cementation.

Well NK1 records 31 Oligocene-to-Early Miocene sea-level fall events and at least nine Quaternary glacial lowstands [12,53]. Two major exposure surfaces at the tops of the Meiji and Liyue formations correspond to significant regional hiatuses of approximately 9.38 Ma and 2.4 Ma, respectively [26]. The variegated limestone layers developed during the late Oligocene to early Miocene indicate multiple exposure events [32], which are associated with regional tectonic events, including Proto-South China Sea subduction, Southwest Sub-basin spreading, and Sabah-Palawan collision, also providing conditions for meteoric diagenesis and dolomitization [26]. In summary, the three identified stages reveal processes of cementation in the Nansha reef: from active marine circulation, through seepage-reflux stage, to marine environments controlled by sea level.

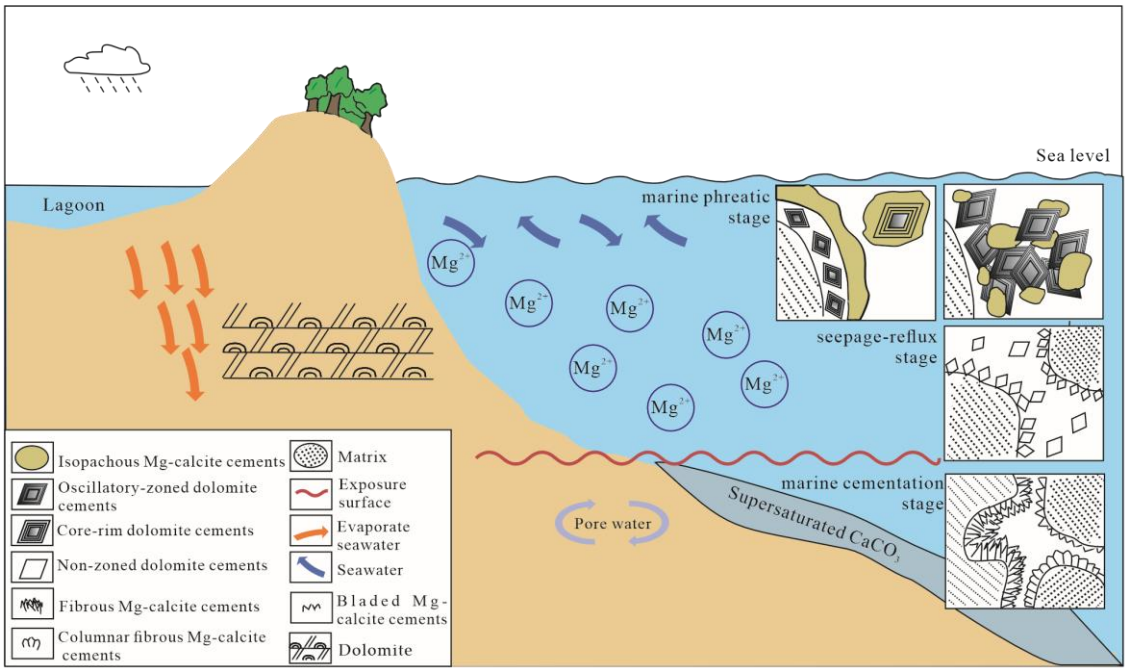


Figure 9. Cementation processes of Cenozoic reef carbonates.

6. Conclusions

1. Reef cements in the Well NK1 are dominated by two main types: magnesian calcite and dolomite. Magnesian calcite cements include four morphological types: fibrous, columnar-fibrous, bladed, and isopachous. Dolomite cements include two types: zoned dolomite and non-zoned dolomite. Zoned dolomite can be further subdivided into core–rim structured dolomite and oscillatory-zoned dolomite.
2. Based on sample observations, fibrous, columnar-fibrous and bladed magnesian calcite cements are mainly developed in the Meiji and Liyue formations; isopachous magnesian calcite and zoned dolomite are mainly developed in the Nansha Formation; non-zoned dolomite is mainly developed in the Yongshu and Nanwan formations.
3. In the Well NK1, isopachous magnesian calcite and zoned dolomite are formed during the marine phreatic stage; non-zoned dolomite are formed during the seepage-reflux stage; and bladed, fibrous, and columnar-fibrous magnesian calcite cements aree formed during the marine cementation stage.

Author Contributions:. Conceptualization, W.Y. and Y.L.; methodology, Y.L. and Z.W.; investigation, Z.W.; data curation, Y.L. and Z.W.; writing—original draft preparation, Z.W.; writing—review and editing, W.Y.; supervision, W.Y.; funding acquisition, W.Y. All authors have read and agreed to the published version of the manuscript.

Funding: This work was supported by the National Key Research and Development Program of China (2021-06).

Data Availability Statement: Data are contained within the article.

Conflicts of Interest: The authors declare no conflicts of interest.

References

1. Tucker, M.E.; Wright, V.P. *Carbonate Sedimentology*; Blackwell Scientific Publications: Oxford, UK, 1990; p. 482. https://doi.org/10.1002/9781444314175.
2. Flügel, E. *Microfacies of Carbonate Rocks: Analysis, Interpretation and Application*, 2nd ed.; Springer: Berlin/Heidelberg, Germany, 2010; p. 984. https://doi.org/10.1007/978-3-642-03796-2.
3. Moore, C.H. Carbonate Reservoirs: Porosity Evolution and Diagenesis in a Sequence Stratigraphic Framework. In *Developments in Sedimentology 55*; Elsevier: Amsterdam, The Netherlands, 2001; p. 444.
4. Jones, B. Microarchitecture of dolomite crystals as revealed by subtle variations in solubility: Implications for dolomitization. *Sediment. Geol.* **2013**, *288*, 66–80. https://doi.org/10.1016/j.sedgeo.2013.01.004.
5. Lucia, F.J. *Carbonate Reservoir Characterization: An Integrated Approach*, 2nd ed.; Springer: Berlin/Heidelberg, Germany, 2007; p. 336. https://doi.org/10.1007/978-3-540-72742-2.
6. Melim, L.A.; Swart, P.K.; Maliva, R.G. Meteoric and marine-burial diagenesis in the subsurface of Great Bahama Bank. *SEPM Spec. Publ.* **2002**, *70*, 137–161. https://doi.org/10.2110/pec.01.70.0137.
7. Braithwaite, C.J.R.; Rizzi, G.; Darke, G. The geometry and petrogenesis of dolomite hydrocarbon reservoirs: Introduction. *Geol. Soc. Lond. Spec. Publ.* **2004**, *235*, 1–6. https://doi.org/10.1144/GSL.SP.2004.235.01.01.
8. Liu, X.M.; Hardisty, D.S.; Lyons, T.W.; Swart, P.K. Evaluating the fidelity of the cerium paleoredox tracer during variable carbonate diagenesis on the Great Bahamas Bank. *Geochim. Cosmochim. Acta.* **2019**, *248*, 25–42. https://doi.org/10.1016/j.gca.2018.12.028.
9. Folk, R.L. The natural history of crystalline calcium carbonate: Effect of magnesium content and salinity. *J. Sediment. Petrol.* **1979**, *44*, 40–53.
10. Longman, M.W. Carbonate diagenetic textures from near surface diagenetic environments. *AAPG Bull.* **1980**, *64*, 461–487. https://doi.org/10.1306/2F918A63-16CE-11D7-8645000102C1865D.
11. Hood, A.S.; Wallace, M.W.; Drysdale, R.N. Neoproterozoic aragonite-dolomite seas? widespread marine dolomite precipitation in Cryogenian reef complexes. *Geology* **2011**, *39*, 871–874. https://doi.org/10.1130/g32119.1.

12. Luo, Y.; Li, G.; Rao, S.Y.; Zhu, X.W.; Xu, W.; Yan, W. Multistage diagenetic fluid shaping miocene island dolostones on one isolated atoll in the south china sea: Insights from la-icp-ms u–pb dating and geochemical characterization. *Minerals* **2024**, *14*, 143. https://doi.org/10.3390/min14020157.
13. Jones, B. Inside-out dolomite. *J. Sediment. Res.* **2007**, *77*, 539–551. https://doi.org/10.2110/jsr.2007.056.
14. Wang, X.L.; Jin, Z.J.; Hu, W.X. Using in situ REE analysis to study the origin and diagenesis of dolomite of Lower Paleozoic, Tarim Basin. *Sci. China Ser. D Earth Sci.* **2009**, *39*, 721–733. (in Chinese with English abstract)
15. Olanipekun, B.J.; Azmy, K.; Brand, U. In situ characterization of dolomite crystals: Evaluation of dolomitization process and its effect on zoning. *Sedimentology* **2017**, *64*, 1708–1730. https://doi.org/10.1111/sed.12371.
16. Eiler, J.M. Paleoclimate reconstruction using carbonate clumped isotope thermometry. *Quat. Sci. Rev.* **2011**, *30*, 3575–3588. https://doi.org/10.1016/j.quascirev.2011.09.001.
17. Roberts, N.M.W.; Rasbury, E.T.; Parrish, R.R.; Smith, C.J.; Horstwood, M.S.A.; Condon, D.J. A calcite reference material for LA-ICP-MS U-Pb geochronology. *Geochem. Geophys. Geosyst.* **2017**, *18*, 2807–2814. https://doi.org/10.1002/2016GC006784.
18. Godeau, N.; Deschamps, P.; Guihou, A.; Leonide, P.; Tendil, A.; Gerdes, A.; Hamelin, B.; Girard, J.P. U-Pb dating of calcite cement and diagenetic history in microporous carbonate reservoirs: Case of the Urgonian Limestone, France. *Geology* **2018**, *46*, 247–250. https://doi.org/10.1130/G39905.1.
19. Wang, Z.F.; Shi, Z.Q.; Zhang, D.J.; Huang, B.; Yu, C.; Yang, X. Microscopic features and genesis for Miocene to Pliocene dolomite in Well Xike-1, Xisha Islands. *Earth Sci. J. China Univ. Geosci.* **2015**, *40*, 633–644. (in Chinese with English abstract) https://doi.org/10.3799/dqkx.2015.050.
20. Liu, X.Y.; Shao, L.; Shi, D.F.; Li, Q.; Qiao, P. Element geochemical characteristics and their relationship with sea level fluctuations in Well Xike-1, Xisha Islands. *Mar. Geol. Front.* **2021**, *37*, 8–17. (in Chinese with English abstract)
21. Zhao, S.; Zhang, D.J.; Liu, L.; Li, Y. Characteristics of diagenesis in Quaternary bioherm-carbonate rocks in Well Xike-1, Xisha sea area, South China Sea. *Earth Sci.* **2015**, *40*, 711–717. (in Chinese with English abstract)
22. Zhu, Y.Z.; Sha, Q.A.; Guo, L.F. *Cenozoic Coral Reef Geology of Yongshu Reef, Nansha Islands*; Science Press: Beijing, China, 1997; pp. 53–116. (in Chinese)
23. Guo, Y.; Deng, W.; Liu, X.; Kong, K.; Yan, W.; Wei, G. Clumped isotope geochemistry of island carbonates in the South China Sea: Implications for early diagenesis and dolomitization. *Mar. Geol.* **2021**, *437*, 106513. https://doi.org/10.1016/j.margeo.2021.106513.
24. Han, X.; Xu, W.H.; Luo, Y.; Li, G.; Yan, W.; Zhu, X. Development characteristics of dolomite in Well NK1, Nansha Islands and preliminary study on genesis mechanism of ferroan dolomite. *J. Trop. Oceanogr.* **2022**, *41*, 74–88. (in Chinese with English abstract)
25. Jia, Y.; Wu, H.; Yan, W.; Zhang, C.; Hu, B.; Zhang, J.; Tian, L.; Deng, C. Rare earth element geochemistry of reef carbonates in the South China Sea since the Miocene: Insights into paleoclimatic significance. *J. Asian Earth Sci.* **2024**, *265*, 106094. https://doi.org/10.1016/j.jseaes.2024.106094.
26. Li, G.; Xu, W.; Luo, Y.; Yan, W.; Zhu, X.; Yi, L. Strontium isotope stratigraphy and LA-ICP-MS U-Pb carbonate age constraints on the Cenozoic tectonic evolution of the southern South China Sea. *GSA Bull.* **2023**, *135*, 271–285. https://doi.org/10.1130/B36365.1.
27. Hall, R. Cenozoic geological and plate tectonic evolution of SE Asia and the SW Pacific: Computer-based reconstructions, model and animations. *J. Asian Earth Sci.* **2002**, *20*, 353–431. https://doi.org/10.1016/S1367-9120(01)00069-4.
28. Sun, Z.; Zhong, Z.; Keep, M.; Zhou, D.; Cai, D.; Li, X.; Wu, S.; Jiang, J. 3D analogue modeling of the South China Sea: A discussion on breakup pattern. *J. Asian Earth Sci.* **2011**, *34*, 544–556. https://doi.org/10.1016/j.jseaes.2008.09.002.
29. Zhao, H.T.; Song, C.J.; Zhu, Y.Z. Geomorphology and modern sedimentary characteristics of coral reefs in the "Dangerous Grounds" of the Nansha Islands. *Quat. Sci.* **1992**, *4*, 368–377. (in Chinese with English abstract)
30. Yi, L.; Deng, C.L.; Xu, X.D.; Yu, H.; Qiang, X.; Jiang, X.; Chen, Y.; Su, T.; Chen, G.; Li, P.; et al. Paleomagnetic and rock magnetic constraints on the stratigraphic framework of reef drilling core NK1, southern South China Sea. *Mar. Geol.* **2021**, *442*, 106645.
31. Su, X.; Xiang, R.; Yi, L.; Zhang, Y.N.; Qin, G.Q.; Yan, W. Neogene carbonate platform development in the southern South China Sea: Evidence from calcareous microfossils. *Palaeogeogr. Palaeoclimatol. Palaeoecol.* **2024**, *638*, 112028. https://doi.org/10.1016/j.palaeo.2024.112093.
32. Cheng, Z.; Wei, K.; Liu, J.; Wang, S.; Li, G.; Xu, W.; Yan, W.; Luo, Y.; Tian, Y.; Wang, M. Genesis geological implications of multicolored reef limestone in the early-middle Miocene Mischief Reef Nansha Islands. *Geol. J.* **2022**, *57*, 3754–3767. https://doi.org/10.1002/gj.4509.
33. Gregg, J.M.; Bish, D.L.; Kaczmarek, S.E.; Machel, H.G. Mineralogy, nucleation and growth of dolomite in the laboratory and sedimentary environment: A review. *Sedimentology* **2015**, *62*, 1749–1769. https://doi.org/10.1111/sed.12202.

34. Scholle, P.A.; Ulmer-Scholle, D.S. A Color Guide to the Petrography of Carbonate Rocks: Grains, Textures, Porosity, Diagenesis. In *AAPG Mem. 77*; AAPG: Tulsa, OK, USA, 2003; p. 474.
35. Zhao, D.F.; Tan, X.C.; Hu, G.; Wang, L.C.; Wang, X.F.; Qiao, Z.F.; Luo, S.C.; Tang, H. Characteristics and primary mineralogy of fibrous marine dolomite cements in the end-Ediacaran Dengying Formation, South China: Implications for aragonite-dolomite seas. *Palaeogeogr. Palaeoclimatol. Palaeoecol.* **2021**, *581*, 110635. https://doi.org/10.1016/j.palaeo.2021.110635.
36. Machel, H.G. Concepts and models of dolomitization: A critical reappraisal. In *The Geometry and Petrogenesis of Dolomite Hydrocarbon Reservoirs*; Braithwaite, C.J.R., Rizzi, G., Darke, G., Eds.; Geological Society, London, Special Publications: London, UK, 2004; Volume 235, pp. 7–63. https://doi.org/10.1144/GSL.SP.2004.235.01.02.
37. Lamothe, K.G.; Wallace, M.W.; Hood, A.V.; Rose, C.V. An earliest Ediacaran oxygenation episode in the Wilpena Group, Adelaide Superbasin, South Australia. *Precambrian Res.* **2024**, *409*, 107433. https://doi.org/10.1016/j.precamres.2024.107433.
38. Vanghi, V.; Frisia, S.; Borsato, A. Genesis and microstratigraphy of calcite coralloids analysed by high resolution imaging and petrography. *Sed. Geo.* **2017**, *359*, 16–28. https://doi.org/10.1016/j.sedgeo.2017.08.001.
39. Zhao, X.Y.; Zheng, Y.C.; Liu, C.; Yang, Z.S.; Dong, Y.R.; Liu, J.C. Magmatic characteristics and oxygen fugacity variations in the Eocene Yulong porphyry copper belt. *Ore Geol. Rev.* **2025**, *178*, 106459.
40. Hood, A.S.; Wallace, M.W. Neoproterozoic marine carbonates and their paleoceanographic significance. *Glob. Planet. Change.* **2018**, *160*, 28–45. https://doi.org/10.1016/j.gloplacha.2017.11.006.
41. Melzer, S.E.; Budd, D.A. Retention of high permeability during shallow burial (300 to 500 m) of carbonate grainstones. *J. Sediment. Res.* **2008**, *78*, 548–561. https://doi.org/10.2110/jsr.2008.060.
42. Wu, S.G.; Yang, Z.; Wang, D.W.; Lü, F.; Lüdmann, T.; Fulthorpe, C.; Wang, B. Architecture, development and geological control of the Xisha carbonate platforms, northwestern South China Sea. *Pet. Explor. Dev.* **2019**, *46*, 233–242. https://doi.org/10.1016/j.margeo.2013.12.016.
43. Wu, F.; Xie, X.N.; Yan, W.; Zhu, Y.H.; Chen, B.C.; Chen, J.N.; Zhou, M. Quaternary evolution of the Meiji Atoll (Mischief Reef) in the southern South China Sea. *Palaeogeogr. Palaeoclimatol. Palaeoecol.* **2023**, *634*, 111912. https://doi.org/10.1016/j.palaeo.2023.111912.
44. Hood, A.S.; Wallace, M.W. Synsedimentary diagenesis in a Cryogenian reef complex: Ubiquitous marine dolomite precipitation. *Sed. Geol.* **2012**, *255*, 56–71. https://doi.org/10.1016/j.sedgeo.2012.02.004.
45. Shuster, A.M.; Wallace, M.W.; van Smeerdijk Hood, A.; Jiang, G.Q. The Tonian Beck Spring dolomite: Marine dolomitization in a shallow, anoxic sea. *Sediment. Geol.* **2018**, *368*, 83–104. https://doi.org/10.1016/j.sedgeo.2018.03.003.
46. Jones, B. Dolomite crystal architecture: Genetic implications for the origin of the Tertiary dolostones of the Cayman Islands. *J. Sediment. Res.* **2005**, *75*, 177–189. https://doi.org/10.2110/jsr.2005.014.
47. Rao, S.; Li, G.; Zhu, X.; Yan, W. Neogene sedimentary evolution of biogenic reefs on an isolated volcanic cone in the southern South China Sea. *Palaeogeogr. Palaeoclimatol. Palaeoecol.* **2025**, *657*, 112588. https://doi.org/10.1016/j.palaeo.2025.112784.
48. Kaczmarek, S.E.; Sibley, D.F. On the evolution of dolomite stoichiometry and cation order during high-temperature synthesis experiments: An alternative model for the geochemical evolution of natural dolomites. *Sediment. Geol.* **2011**, *240*, 30–40. https://doi.org/10.1016/j.sedgeo.2011.07.003.
49. Hood, A.S.; Wallace, M.W. Extreme ocean anoxia during the Late Cryogenian recorded in reefal carbonates of Southern Australia. *Precambrian Res.* **2015**, *261*, 96–111. https://doi.org/10.1016/j.precamres.2015.02.008.
50. Wallace, M.W.; Hood, A.S.; Fayle, J.; Hordern, E.S.; O'Hare, T.F. Neoproterozoic marine dolomite hardgrounds and their relationship to cap dolomites. *Precambrian Res.* **2019**, *328*, 269–286. https://doi.org/10.1016/j.precamres.2019.04.026.
51. Kaczmarek, S.E.; Sibley, D.F. Direct physical evidence of dolomite recrystallization. *Sedimentology* **2014**, *61*, 1862–1882. https://doi.org/10.1111/sed.12119.
52. Kim, J.; Kimura, Y.; Puchala, B.; Yamazaki, T.; Becker, U.; Sun, W. Dissolution enables dolomite crystal growth near ambient conditions. *Science* **2023**, *382*, 915–920. https://doi.org/10.1126/science.adi3690.
53. Sun, Y.B.; Zhang, Y.F.; Tang, Y.; Wang, Z.Y.; Yan, W.; Xu, W.H.; Qu, H.Z.; Xi, A.H. Early Oligocene gravity-flow deposits at the base of the Meiji Reef system in the South China Sea, and their palaeoclimate significance. *Palaeogeogr. Palaeoclimatol. Palaeoecol.* **2023**, *623*, 111621. https://doi.org/10.1016/j.palaeo.2023.111621.

Disclaimer/Publisher's Note: The statements, opinions and data contained in all publications are solely those of the individual author(s) and contributor(s) and not of MDPI and/or the editor(s). MDPI and/or the editor(s) disclaim responsibility for any injury to people or property resulting from any ideas, methods, instructions or products referred to in the content.